# Regulatory Roles of the N-Terminal Domain Based on Crystal Structures of Human Pyruvate Dehydrogenase Kinase 2 Containing Physiological and Synthetic Ligands[†,‡]

Thorsten R. Knoechel,[⊥,§] Alec D. Tucker,[⊥] Colin M. Robinson,[⊥] Chris Phillips,[⊥] Wendy Taylor,[⊥] Peter J. Bungay,[⊥] Shane A. Kasten,[#] Thomas E. Roche,[#] and David G. Brown*[,⊥]

*PGRD Sandwich, Pfizer Ltd, Sandwich, Kent CT139NJ, United Kingdom, and Department of Biochemistry, Kansas State University, Manhattan, Kansas 66506*

*Received July 19, 2005; Revised Manuscript Received October 30, 2005*

ABSTRACT: Pyruvate dehydrogenase kinase (PDHK) regulates the activity of the pyruvate dehydrogenase multienzyme complex. PDHK inhibition provides a route for therapeutic intervention in diabetes and cardiovascular disorders. We report crystal structures of human PDHK isozyme 2 complexed with physiological and synthetic ligands. Several of the PDHK2 structures disclosed have C-terminal cross arms that span a large trough region between the N-terminal regulatory (R) domains of the PDHK2 dimers. The structures containing bound ATP and ADP demonstrate variation in the conformation of the active site lid, residues 316−321, which enclose the nucleotide $\beta$ and $\gamma$ phosphates at the active site in the C-terminal catalytic domain. We have identified three novel ligand binding sites located in the R domain of PDHK2. Dichloroacetate (DCA) binds at the pyruvate binding site in the center of the R domain, which together with ADP, induces significant changes at the active site. Nov3r and AZ12 inhibitors bind at the lipoamide binding site that is located at one end of the R domain. Pfz3 (an allosteric inhibitor) binds in an extended site at the other end of the R domain. We conclude that the N-terminal domain of PDHK has a key regulatory function and propose that the different inhibitor classes act by discrete mechanisms. The structures we describe provide insights that can be used for structure-based design of PDHK inhibitors.

In energy metabolism, pyruvate is a central intermediate in carbohydrate degradation. Under anaerobic conditions, it is reduced to lactate, while under aerobic conditions it is decarboxylated and converted into acetyl-coenzyme A, which serves as an activated C-2 source for the citric acid cycle or fatty acid synthesis. The irreversible decarboxylation of pyruvate is catalyzed by the pyruvate dehydrogenase multienzyme complex (PDC),[1] a macromolecular assembly (5−10 million Da) of multiple copies of three catalytic components: pyruvate dehydrogenase (E1), dihydrolipoyl acetyltransferase (E2), and dihydrolipoyl dehydrogenase (E3). In addition, mammalian PDC contains an E3-binding protein (or protein X) and two associated regulatory enzymes, PDH kinase (PDHK) and PDH phosphatase (PDP) (*1*, *2*). Reversible phosphorylation occurs at three serine residues of the E1 component and downregulates PDC activity (*1*−*6*). Efficient phosphorylation of E1 is facilitated by noncovalent binding of PDHK to the lipoyl domains of the E2 oligomer, particularly the inner lipoyl domain (L2) of E2 (*2*, *7*−*13*). Binding requires the lipoyl prosthetic groups, and reduction and acetylation of the lipoyl groups of E2 enhance PDHK activity (*2*, *13*−*18*). At least four PDHK isozymes and two PDP isozymes are involved in the tissue and metabolic state specific control of the PDC activity (*2*, *19*−*29*).

PDHK together with the branched-chain α-ketoacid dehydrogenase kinase (BCK) form a class of mitochondrial protein kinases (mPK's) that are unrelated to the major class of eukaryotic protein kinases but are similar to the histidine protein kinases found in prokaryotes (*19*−*20*, *30*−*34*). These proteins form dimers (*11*, *12*, *33*, *34*), each consisting of an N-terminal domain with a four-helix bundle topology, and a C-terminal ATP-binding domain, and belong to the GHKL superfamily (*31*, *32*, *35*−*41*). This work provides new structural insights into the N-terminal regulatory domain and the location of novel regulatory binding sites.

[†] This work was supported by Pfizer Ltd, by National Institutes of Health Grant DK18320 to TER, and by KSU Agricultural Experiment Station (Contribution 05-325-J).

[‡] All crystallographic atom coordinates described in this paper have been deposited with the Protein Data Bank (entries 2btz, 2bu2, 2bu5, 2bu6, 2bu7, and 2bu8).

* To whom correspondence should be addressed. Pfizer Ltd, PGRD Sandwich ipc 636, Sandwich, Kent CT13 9NJ, United Kingdom. Tel.: +44 (0)1304 648466. Fax: +44 (0)1304 651820. E-mail: david.g.brown@pfizer.com.

[⊥] Pfizer Ltd.

[#] Kansas State University.

[§] Present address: Protein Crystallography (ZD-A/ZFA) Merck KGaA, Frankfurter Strasse 250, D-64293 Darmstadt, Germany.

[1] Abbreviations: PDC, pyruvate dehydrogenase complex; E1, pyruvate dehydrogenase component; E2, dihydrolipoyl acetyltransferase component; L2 domain, interior lipoyl domain of E2; E3, dihydrolipoyl dehydrogenase; PDHK, pyruvate dehydrogenase kinase; DCA, dichloroacetate; BCK, branched-chain α-ketoacid dehydrogenase kinase; mPK's, mitochondrial protein kinases; Cat domain, C-terminal catalytic domain of PDHK2; R domain, N-terminal regulatory domain of PDHK2; Nov3r, (4-{(2,5)-dimethyl-4-[3,3,3-trifluoro-2-hydroxy-2-methylpropanoyl]piperazinyl}carbonyl)benzonitrile; Pfz3, methyl {3-chloro-4-[(4-isopropylbenzyl)oxy]phenyl}acetate; AZ12 (*N*-{4-[(ethylanilino)sulfonyl]-2-methylphenyl}-3,3,3-trifluoro-2-hydroxy-2-methylpropanamide).

10.1021/bi051402s CCC: $33.50 
Published on Web 12/20/2005

Dichloroacetate (DCA) is a well-established activator of PDC (*42*, *43*), but one that causes toxic side effects (*44*, *45*). Pharmacological studies indicate that DCA-facilitated increases in PDC activity have beneficial effects in several metabolic and cardiovascular disorders, including diabetes, myocardial ischemia, lactic acidosis, and premature muscle fatigue (*43*, *46*−*51*). The activation of PDC by DCA results from DCA inhibiting PDHK activity by binding at the pyruvate site (*42*, *52*). Given the beneficial effects of DCA, development of inhibitors of PDHK (*53*−*60*) has become a focus of the pharmaceutical industry. We clarify the nature of the sites of binding of some of these inhibitors and introduce a new class of inhibitor.

We have determined the X-ray structure of human PDHK2 in the presence and in the absence of physiological and synthetic ligands.[2] Changes induced in PDHK2 structure with binding of ligands correlate with changes in the regulation of PDHK2 function (*6*, *22*, *61*−*63*). We discuss the interactions that contribute to dimer formation and compare them with the recently disclosed structure of the human PDHK3 isoform complexed with the L2 domain of E2 (*64*). The structures of complexes of human PDHK2 with ligands bound at the various sites can be utilized for structure-based design of novel PDHK inhibitors.

## EXPERIMENTAL PROCEDURES

*Cloning, Protein Expression, and Purification.* Human PDHK2 (GenBank Accession number L4245; *19*) residues A8-T399 was cloned into pFastbac1 (Invitrogen) with a N-terminal His6 tag and thrombin cleavage site, using PCR. Recombinant baculovirus was generated using the Bac-to-Bac baculovirus expression system (Invitrogen). The protein was expressed by infection of *T.ni* High5 insect cells with recombinant baculovirus in Applikon 3 L fermenters using Excel 405 media (JRH biosciences) at a cell density of $2 \times 10^6$ cells/mL and MOI = 2. The fermentation was harvested 72 h post infection. The frozen cell pellet was lysed in 50 mM Tris-HCl (pH 8), 150 mM sodium chloride, 10 mM imidazole, 5 mM $\beta$-mercaptoethanol, containing EDTA free protease inhibitor cocktail tablets (Roche). Cell breakage was achieved using continuous homogenization (Constant systems). Following centrifugation of the sample, the supernatant was loaded onto nickel-NTA Superflow resin (Qiagen). The protein was step eluted using 500 mM imidazole, and buffer was exchanged immediately into 20 mM Tris-HCl (pH 8.0), 150 mM sodium chloride, and 2.5 mM $CaCl_2$ (cleavage buffer). The hexa-histidine tag was removed by thrombin (Sigma) cleavage, using a concentration of 5 NIH units/mg of protein for 3 h at 25 °C. Postcleavage the protein was applied onto nickel-NTA Superflow resin (Qiagen), and the flow-through was collected. Fractions were pooled and concentrated to 2 mg/mL before loading onto a Sephacyl-200 (Amersham Biosciences) size exclusion column, using buffer, 20 mM Tris-HCl (pH 8.0), 150 mM sodium chloride, and 1 mM DL-dithiothreitol. Eluted PDHK2 was then stored at −80 °C prior to crystallization.

[2] The atomic coordinates described in this paper have been deposited with the Protein Data Bank (entries 2btz, 2bu2, 2bu5, 2bu6, 2bu7, and 2bu8). The original crystal structures were disclosed in Robinson, C. M., Taylor, W. E., Tucker, A. D., and Knoechel, T. G. Crystal structure of pyruvate dehydrogenase kinase 2 (PDHK-2) and use thereof in methods for identifying and designing new ligands, Pfizer, Patent application: EP1247860, 1-304, 2002.

*Crystallization*. Human PDHK2 was concentrated to 10 mg/mL using 10 kDa centrifugal concentrators (Vivascience) at 3000 rpm, 4 °C. Crystallization trials were carried out using hanging drop vapor diffusion at 4 °C. PDHK2 crystallized in a range of conditions with the largest crystals grown from 100 mM sodium acetate pH 5.6−5.8, 6−9% 2-propanol, and 75−125 mM magnesium chloride. Crystals appeared overnight and continued to grow for up to 2 weeks. Crystals display a symmetry of $P6_4$ with cell dimensions $a = b = 109.3$ Å, $c = 85.1$ Å, $\alpha = \beta = 90°$ $\gamma = 120°$. They contained one molecule per asymmetric unit (Mw = 44.6 kDa) and had a solvent content of 62%.

Crystals of human PDHK2 in complex with Nov3r (4-{(2,5)-dimethyl-4-[3,3,3-trifluoro-2-hydroxy-2-methylpropanoyl]piperazinyl}carbonyl)benzonitrile; *55*) were obtained by mixing Nov3r at 3-fold molar excess before concentration to 10 mg/mL. Crystallization conditions for complexes of PDHK2 were similar to those reported for the unliganded enzyme. The liganded PDHK2 also yielded crystals in 100 mM MES pH 6.0, 10% 2-propanol, and 200 mM calcium acetate.

Crystals of PDHK2 in complex with AZ12 (*N*-{4-[(ethylanilino)sulfonyl]-2-methylphenyl}-3,3,3-trifluoro-2-hydroxy-2-methylpropanamide); example 12 in patent application WO 99/62873) and Pfz3 (*N*-(2-aminoethyl)-2-{3-chloro-4-[(4-isopropylbenzyl)oxy]phenyl}acetamide) were prepared by soaking crystals of unliganded PDHK2 in stabilizing solution containing the inhibitor at 1 mM concentration. Crystals of human PDHK2 in complex with ATP were obtained by soaking crystals, grown in the presence of Nov3r, in stabilizing solution containing 10 mM ATP. Crystals of human PDHK2 in complex with ADP and DCA were obtained by soaking crystals of unliganded PDHK2 in stabilizing solution containing both ADP and DCA at 10 and 100 mM concentration, respectively.

*Data Collection, Structure Determination, and Refinement*. In all cases, data collection was carried out at 100 K. Protein crystals were flash-frozen at 100 K using a cryo-protection buffer consisting of stabilizing solution and 30−35% glycerol. The structure of recombinant PDHK2 was solved by multiple isomorphous replacement using three heavy atom derivatives. Mercury, iridium, and osmium derivatives were prepared by soaking crystals for 16−18 h in a stabilizing solution (9% 2-propanol in 100 mM sodium acetate buffer at pH 5.8) containing 1 mM ethylmercury thiosalicylate, 5 mM $K_2IrCl_6$, or 10 mM $K_2OsCl_6$, respectively.

X-ray diffraction data of the native protein were collected with an ADSC Quantum 4 CCD-detector at station 9.6 ($\lambda = 0.8700$ Å) of the Synchrotron Radiation Source (SRS) Daresbury, UK. The diffraction data for the heavy atom derivatives were collected with Rigaku RAXIS-2 or RAXIS-4 image plate detectors on laboratory rotating anode generators using CuK$\alpha$ radiation. All data were processed using the HKL package (*65*). Data collection statistics are summarized in Table 1.

Heavy atom derivative data were scaled to native data with SCALEIT (*66*). Difference Patterson and difference Fourier analysis identified initial heavy atom positions. Refinement of the heavy atom parameters and phase calculation was performed with SHARP (*67*). Phases were improved by 120 cycles of solvent flattening with SOLOMON (*68*). The

Table 1: Data Collection and Phasing Statistics

| | native | EMTS 1 mM | $K_2IrCl_6$ 5 mM | $K_2OsCl_6$ 10 mM | ATP/ compound **1** | compound **1** | compound **2** | compound **3** | ADP/ DCA |
|---|---|---|---|---|---|---|---|---|---|
| resolution [Å] | 2.2 | 2.8 | 3.0 | 2.8 | 2.4 | 2.35 | 2.4 | 2.4 | 2.5 |
| unique reflections | 28844 | 14054 | 11314 | 14047 | 21971 | 23185 | 21614 | 21046 | 20370 |
| completeness [%] | 97.9 | 99.0 | 100.0 | 99.7 | 98.5 | 97.6 | 97.1 | 94.3 | 99.2 |
| redundancy | 3.7 | 7.0 | 8.3 | 8.7 | 3.4 | 2.9 | 3.8 | 7.3 | 3.5 |
| refln $< 3\sigma$ [%] | 90.9 | 88.8 | 90.7 | 90.1 | 79.7 | 83.3 | 87.0 | 87.7 | 84.7 |
| $R_{sym}$[a] | 0.035 | 0.079 | 0.060 | 0.062 | 0.054 | 0.048 | 0.061 | 0.060 | 0.043 |
| $R_{iso}$[b] | | 0.234 | 0.285 | 0.237 | | | | | |
| $R_{cullis}$[c] | | 0.760 | 0.825 | 0.891 | | | | | |
| no. of sites | | 5 | 3 | 5 | | | | | |
| phasing power[d] | | | | | | | | | |
| isomorphous[e] | | 1.51/1.21 | 1.43/1.37 | 1.23/1.06 | | | | | |
| anomalous[f] | | 1.49 | 1.64 | 1.36 | | | | | |

[a] $R_{sym} = \sum_{hkl}\sum_i|I_i(hkl) - \overline{I(hkl)}|/\sum_{hkl}\sum_i|I_i(hkl)|$. [b] $R_{iso} = \sum_{hkl}||F_{PH}(hkl)| - |F_P(hkl)||/\sum|F_P(hkl)|$. [c] $R_{cullis} = \langle$phase integrated lack of closure$\rangle/\langle|F_{PH} - F_P|\rangle$. For centric reflections only. [d] Phasing power $= \langle\{|FH(calc)|/$phase-integrated lack of closure$\}\rangle$. [e] Pairs of values are given for acentric and centric reflections, respectively. [f] For acentric reflections only.

Table 2: Data Refinement Statistics

| | native | ATP/compound 1 | compound 1 | compound 2 | compound 3 | ADP/DCA |
|---|---|---|---|---|---|---|
| resolution range, Å | 30.0−2.2 | 30.0−2.4 | 30.0−2.35 | 30.0−2.4 | 30.0−2.4 | 30.0−2.5 |
| amino acid residues, no. | 356 | 357 | 351 | 352 | 357 | 358 |
| water molecules, no. | none | 91 | 111 | 60 | 153 | 151 |
| ligand molecules | none | ATP, $Mg^{2+}$, compound 1 | compound 1 | compound 2 | compound 3 | ADP, $Mg^{2+}$, DCA |
| rmsd bond length, Å | 0.008 | 0.009 | 0.008 | 0.008 | 0.009 | 0.010 |
| rmsd bond angles, ° | 1.290 | 1.635 | 1.342 | 1.309 | 1.356 | 1.295 |
| R-factor | 0.267 | 0.238 | 0.237 | 0.247 | 0.211 | 0.248 |
| free R-factor (5% of data) | 0.297 | 0.247 | 0.255 | 0.261 | 0.241 | 0.262 |

[a] $R = \sum_{hkl}||F_{obs}| - k|F_{calc}||/\sum_{hkl}|F_{obs}|$.

resulting map was of good quality and used to trace about 75% of the structure using QUANTA (*69*).

Refinement was carried out in the resolution range 30−2.2 Å using CNX (*70*) with the "*mlhl*" maximum likelihood target function. During refinement, model phases were combined with the experimental phase probability distributions provided by SHARP. Partial structure factors from a flat bulk-solvent model and anisotropic B-factor correction were supplied throughout the refinement. The R-factor for the current model is 0.267 (free R-factor, 5% of data, 0.297) for all data in the resolution range 30−2.2 Å. The refinement statistics are summarized in Table 2 (see end of Example section).

The current model contains 355 out of 394 residues present in the construct and is well defined in most regions of the polypeptide chain. The electron density is weak for residues 32−35, 65−71, 97−101, 302−304, and 367−384. No interpretable electron density was observed for residues 170−177, 305−310, and 385−399. The latter are not included in the model, and residues 378−379 are modeled as alanine.

Diffraction data of PDHK2 in complex with Nov3r, AZ12, and both ATP and Nov3r were collected with an ADSC Quantum 4 CCD-detector at beamline ID14-2 ($\lambda = 0.9326$ Å) of the European Synchrotron Radiation Facility (ESRF), Grenoble, France. Diffraction data of human PDHK2 in complex with Pfz3 were with a Rigaku RAXIS-2 image plate detector on a laboratory rotating anode generator using Cu Kα radiation. Diffraction data of PDHK2 in complex with both ADP and DCA were collected with an ADSC Quantum 4 CCD-detector at station 9.6 ($\lambda = 0.87$ Å) of the SRS. Data processing was carried out with the HKL program package (*65*). Data collection statistics are summarized in Table 1.

The structures were determined by difference Fourier methods using the unliganded human PDHK2 structure to calculate model phases and subsequently refined using CNX (*70*). Interactive graphical model building was carried out with QUANTA (*69*). In all structures, the respective ligands were clearly defined by the initial electron density maps. For a summary of refinement statistics, see Table 2.

*PDHK Activity Assay.* Compounds were assessed for inhibition of PDHK in an assay adapted from Espinal et al. (*53*). In the first part of the assay, compounds were incubated with porcine PDC (Sigma P-7032) and MgATP, and the reaction was stopped after defined intervals. In the second part of the assay, the residual PDC activity was measured by monitoring the rate of reduction of NAD at 340 nm.

The assay was performed in flat-bottom 96-well microtiter plates, using a final volume of 50 μL for the first part of the assay (kinase reaction), and 250 μL for the PDC reaction. At first, 10 μL of test compound in a suitable diluent, 20 μL of kinase buffer (20 mM potassium phosphate, pH 7.0, 4 mM $MgCl_2$, 4 mM dithiothreitol) and 10 μL of PDC (Sigma, P-7032, diluted with water to a final concentration of 1.83 mg/mL) were mixed and incubated for 10 min; then 10 μL of ATP solution (125 μM in kinase buffer) was added to start the reaction. The incubations were carried out at 30 °C. The kinase reaction was terminated after defined intervals (usually 0, 10, 20, 30, 60, and 90 min) by initiating the PDC reaction. This was done by addition of 200 μL of PDC substrate solution (1 mM thiamine pyrophosphate, 0.5 mM NAD, 0.5 mM coenzyme A, 12 mM pyruvate, 5 mM dithiothreitol). Kinetic readings were taken at 340 nm conducted at 12 s intervals for 20 min with shaking for 1 s before each reading, in a SpectraMax plate reader. The data were processed using the Spectramax software.

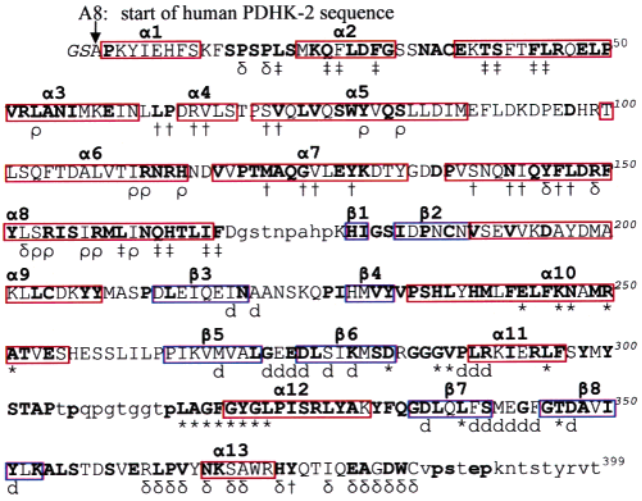


FIGURE 1: Sequence of mature human PDHK2 construct used for crystallization. The sequence of mature human PDHK2 starts with residue Ala8; the sequence numbering lacks eight amino acids from the leader sequence. The two preceding residues (Gly6 and Ser7) are part of the engineered thrombin cleavage site, linking the construct to the hexahistidine tag. Secondary structural elements are indicated by a box (helices in red, strands in blue) and labeled. Residues conserved in all four PDHK isozymes in bold; excluding the interdomain linker (residues 170−177), this includes 50% of the residues in the regulatory domain (residues 8−169) and 48% of residues in the catalytic domain (residues 178−399). The following designations are used: (*) for residues in contact with ATP; (‡) for residues in contact with Nov3r (UK-403,658); ($\rho$) for residues in contact with DCA; (†) for residues in contact with Pfz3; (d) for residues involved in the main dimer interface; ($\delta$) for residues involved in C-terminal cross arm dimer interaction. Residues in lower case are disordered in the structure of the native enzyme.

## RESULTS AND DISCUSSION

*General Structure of Human PDHK2 Subunit*. The structure of human PDHK2 (Figure 2A), displays the same general fold as rat PDHK2 and rat BCK (*33*, *34*), with which the mature human PDHK2 shares 97 and 27% (108/399 residues) sequence identity, respectively. Figure 1 shows the relationship of the sequence to the secondary structure elements as well as the location of residues involved at various functional regions considered, below. These include secondary and other structure elements not described in rat PDHK2. Figure 1S (Supporting Information) shows the aligned sequences of four human PDHK; the numbering in all cases starts with mature protein and that numbering is used throughout this text. The overall topology of human PDHK2 is similar to that described for rat PDHK2 and human PDHK3 (*33*, *64*) with some ligand induced variations which will be discussed.

Because of the established catalytic role of the C-terminal domain, this work focuses on the regulatory role of the N-terminal domain. The domains will be referred to as the Cat domain and the R domain, respectively. The association of the R and Cat domains produces an extended cavity (Figure 2B) with a long central groove spanning >25 Å and the outer edges (e.g., helices 7 to 9) separated by ~30 Å. The active site in the Cat domain is located toward one end of the wide cavity with the $\gamma$-phosphate of ATP located next to the groove. The active site side of each domain (and subunit) with its thick wedge-shaped cavity opening will be referred to as the *substrate-binding face*; the opposite sides of each will be termed its *dimerization face*.

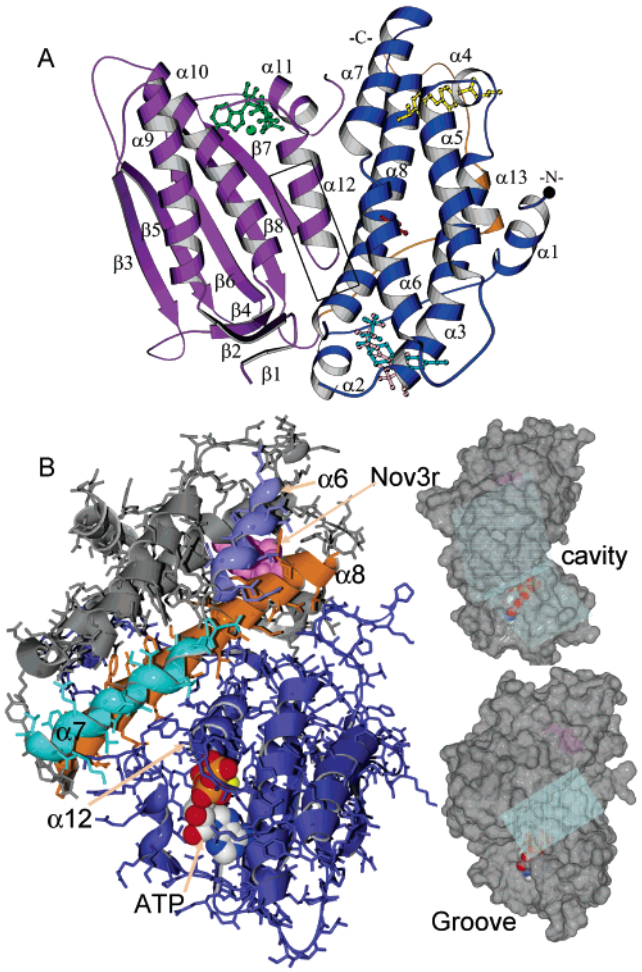


FIGURE 2: Ribbon diagram with location of inhibitors and wedge/groove region of PDHK2 subunit. Panel A shows ribbon representation of the human PDHK2 monomer structure with numbered secondary structure and bound ligands as ball-and-stick models: ATP/$Mg^{2+}$ in green; Nov3r in cyan; AZ12 in pink; DCA in red; Pfz3 in yellow. The N-terminal regulatory domain (R domain) is shown in blue, the C-terminal catalytic (Cat) domain in purple and the C-terminal extension in orange in panel A. Panel B on left shows bound ATP (CPK representation) and Nov3r (magenta) in a space-filled presentation in a strands/stick side chain presentation of the PDHK2 subunit; the same subunit as surface structures, shown on the right, emphasizes the active site cavity (upper) and groove (lower) shapes at active site region of PDHK2 subunit. In the left structure, the Cat domain is dark blue and in general the R domain is gray but helices 6, 7, and 8 are blue, cyan, and orange, respectively. In structures in panel B, the C-terminal extension is not included. The location of a groove between the regulatory and catalytic domains is indicated by a rectangle in panel B.

*Interactions Supporting the PDHK2 Dimer*. The PDHK isozymes form homodimers as well as heterodimers (*11*, *12*, *33*, *71*). The crystal structure of human PDHK2 forms a crystallographic dimer (Figure 3A,C, PDHK2), which is consistent with solution studies (*12*) and similar to the rat PDHK2, BCK, and PDHK3·L2 structures (*33*, *34*, *64*) (Figure 3B). The main contacts between the monomers are formed by the central $\beta$-sheets of the dimerization face ($\beta$3, $\beta$5, $\beta$6, $\beta$8, and $\beta$7) of the Cat domain (residues labeled with d in Figure 1). Besides $\beta$-strand intersubunit interactions, residues in helix α11 contribute to dimer formation by interacting with the loop connecting $\beta$5 to $\beta$6.

The dimerization faces of the two R domains form an oblique open-ended trough. Dimer interactions similar to

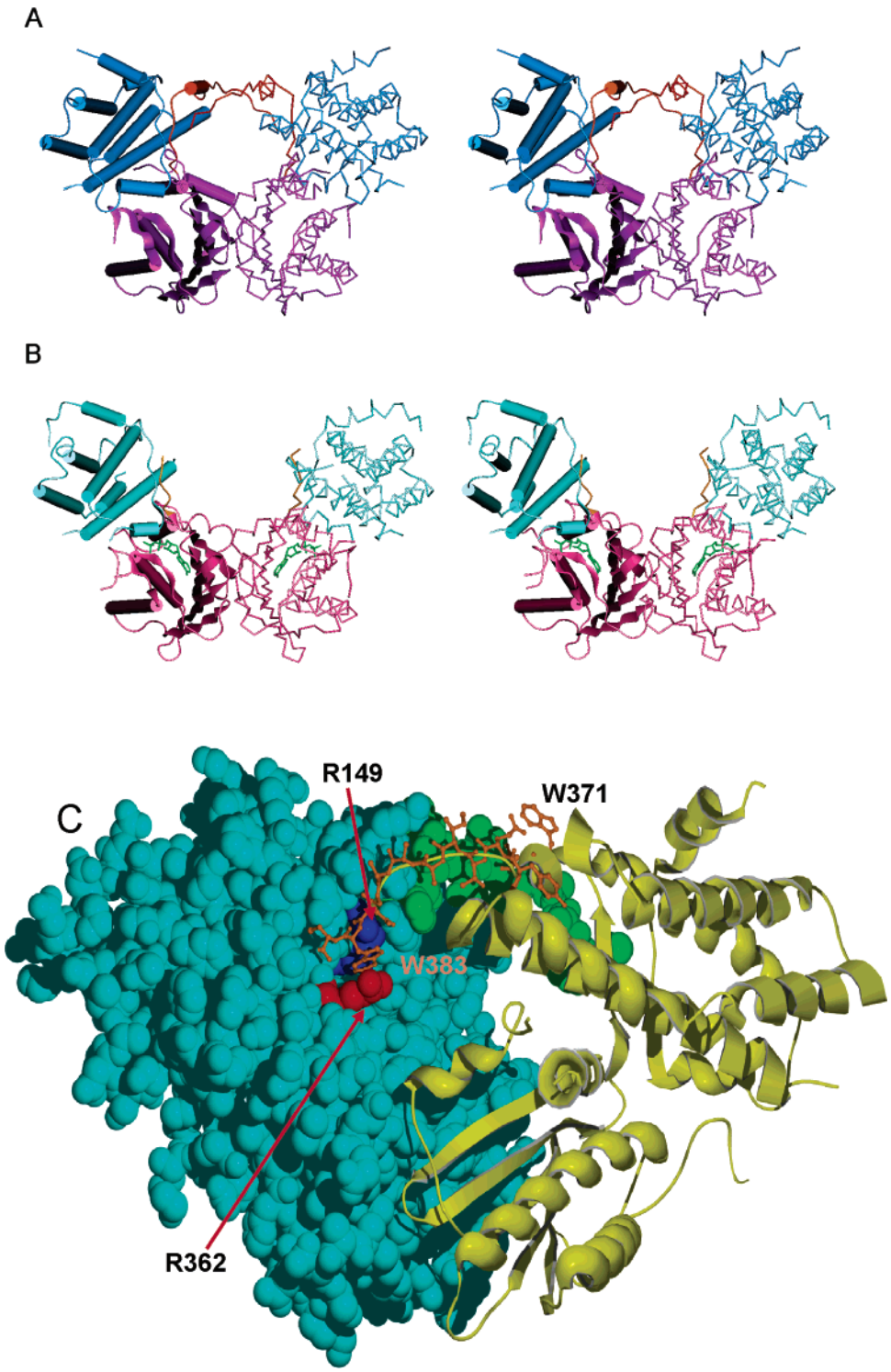


FIGURE 3: Stereo illustration of the human PDHK2 dimer assembly with (A) and without (B) the intersubunit cross arm and anchoring of the cross arm structure. In panels A and B, the left subunit shows the secondary structure topology and the right is the symmetry related backbone in strand format. Panels A and C show apo PDHK2 with C-terminal cross arm. Panel B shows the stereoview of the rat PDHK2 dimer with bound ADP (green), in an orientation that optimizes the superposition of the C-terminal regulatory domains in panel A. Panel C shows Trp383 from right subunit cross arm (orange stick structure) anchored between Arg149 (blue) and Arg362 (red) of the left subunit (cyan with green cross arm in space filled format).

those observed in the PDHK3·L2 structure (*64*) were revealed in the apo and Nov3r and AZ12 liganded human PDHK2 structures (Figure 3A,C). These were not present in the rat PDHK2 structure with ADP bound (Figure 3B) or the human PDHK structure with ADP and DCA bound. C-terminal residues 361−384 of each subunit, including helix α13, form a structure that extends from the Cat domain of one monomer across the dimerization face of its cognate R domain and then spans the intersubunit trough to interact with the dimerization face of the R domain of the symmetry related second subunit (Figure 3A,C; key interacting residues labeled with $\delta$ in Figure 1 for both domains). The end of the cross arm is anchored by interactions of residues 382−384 with Trp383 playing the most important role. As shown

in Figure 3C, Trp383$\beta$ (orange stick structure from right subunit) is inserted between Arg149α (blue) and Arg362α (red) of the other subunit (left, cyan) at the end of the cross arm interaction. Trp383$\beta$ also interacts with nonpolar α-subunit side chains (Leu152, Leu363, Pro364, and Val365). Asp382$\beta$ side chain makes an important electrostatic interaction with Trp383$\beta$ indole ring and an H-bond with the Tyr145α hydroxyl group. The carbonyl group of Asp382$\beta$ forms H-bonds with the Arg149α side chain and an H-bond with N−H of Val365α. Cys384$\beta$ SH and backbone NH hydrogen bond to the carbonyl group of Leu363α. Between the two cross arms an H-bond interaction is formed between Ile377 and an N−H Arg372 side chain. In the L2 binding PDHK3, the residues equivalent to Arg372 and Glu379 form an inter-cross arm electrostatic interaction; this was not found in human PDHK2 structures; indeed, the Glu379 as well as Gln380 side chains were not resolved (Ala inserted in pdb). From mutational substitution, it is clear that only a very small rotation at Glu379 is required to form the electrostatic interaction with Arg372.

Figure 2S (Supporting Information) shows that the positioning of a cross arm in PDHK2 and PDHK3 are very similar even though PDHK2 was not interacting with the L2 domain. Beyond the cross arm described here, additional C-terminal residues (corresponding to PDHK2 residues 385−395) were found to engage in lipoyl domain and lipoyl group binding in PDHK3·L2 structures (*64*). Our results demonstrate that binding to the L2 domain is not required for cross arm formation. Of the 28 residues involved in forming or stabilizing the C-terminal cross arm connection (red residues and Tyr374 in Figure 1S, Supporting Information), 16 are conserved, and all but three of the remaining conservatively substituted in the other three PDHK isoforms. That supports the hypothesis that these interactions are biologically significant in each of the four PDHK isoforms.

Under two different crystallization conditions, there was no cross arm resolved with ADP bound. That was found with the rat PDHK2·ADP (*33*) and human PDHK2·ADP·DCA crystal structures. In rat PDHK2 structure, the width of the trough between the dimerization faces increases (Figure 3B) and the cavity in the substrate-binding face decreases without the cross arm. In comparison to Apo PDHK2, the distances between the same residue on opposite R domains along the dimerization surfaces is increased with ADP bound by 3 to 9 Å. Using α and $\beta$ to designate the two subunits, there is 7 Å increase between αCs of α and $\beta$ subunits between sets of Gln103 or Glu65 and 5.5 Å increase between Tyr145-αC; this increase is apparent in comparing panels A and B in Figure 3. The spacing at the outer center of the substrate-binding cavity is decreased; for instance, the distance from Leu202 in helix α9 to Leu127 in helix α7 decreased by 4.4 Å with ADP bound. These results indicate that there is a hinge movement between the Cat and R domains of PDHK2 with some degree of twist. Kato et al. (*64*) noted a similar conformational change comparing the rat PDHK2·ADP and PDHK3·L2 structures. They proposed that the change was due to PDHK3 binding the L2 domain. However, our results indicate that the closing of the trough region with concomitant opening of the active site cavity is probably due to forming the cross arm connection and occurs without binding of the L2 domain.

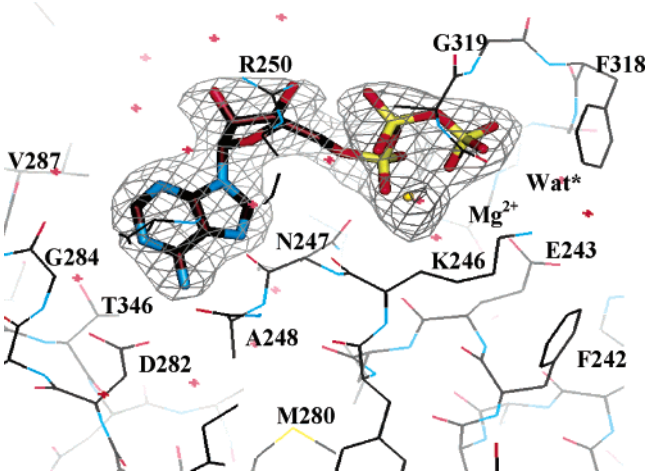


FIGURE 4: ATP/$Mg^{2+}$ together with coordinating water molecules at the ATP binding site of human PDHK2. The model is superimposed onto the $(f_{obs} - f_{calc})\alpha_{calc}$ electron density map at 2.4 Å (contour level: 2.5$\sigma$) calculated prior to incorporation of the complex in the model. A water molecule suggested to occupy the position of the Ser hydroxyl-group in the phosphoryl-transfer reaction is indicated (Wat*).

These same effector conditions (ADP, ADP plus DCA, and ADP plus pyruvate) hinder binding of the PDHK2 to the L2 domain (*12*, *72*)[3] and markedly decrease fluorescence of Trp383.[3] Hiromasa et al.[3] have emphasized that both the ligand-induced increase in Trp383 fluorescence quenching and reduced binding to the L2 domain could result from ligands inducing reversible release of the cross arm interaction; ADP plus pyruvate had the largest effects. These ligands do not cause a similar large decrease in the Trp fluorescence of the PDHK3 isoform or greatly weaken binding of PDHK3 to the L2 domain,[3] which is consistent with retention of the cross arm and L2 binding with ADP bound (*64*). While differences in the different crystal environments may contribute to differences between rat and human PDHK2, large and reciprocal structural changes associated with the separation of the R domain dimerization faces and linked changes in the opening of the substrate binding cavity likely play critical roles in PDHK2 function and regulation. Specifically, the marked inhibition of PDHK2 activity by ADP plus pyruvate may, in part, involve reducing binding to the L2 domain and decreasing the cavity size in the active site which may affect binding of the E1 substrate.

*The ATP Binding Site*. The structure of human PDHK2 was determined in the presence of ATP (Figure 4). The ATP binding pocket is located between the central $\beta$-sheet and the adjacent layer of helices. It is formed from α10, $\beta$7, α11, α12, $\beta$8, and $\beta$9. Upon binding of ATP/ADP, the C-terminal end of the disordered segment between helices α11 and α12 (residues 305−319) becomes ordered with residues 315−322 forming a "lid" with varied interactions with the phosphate groups of ATP and ADP (below) that may be influenced by the binding of other ligands.

[3] Hiromasa, Y., Hu, L., and Roche, T. E. Ligand-induced effects on pyruvate dehydrogenase kinase isoform 2, manuscript submitted. ADP + DCA or pyruvate cause major quenching in tryptophan fluorescence of PDHK2 (primarily involving Trp383) and also cause a marked decrease binding of PDHK2 to GST-L2 (glutathione-*S*-transferase-L2) dimer. Ligands dislodge Trp383 from its anchoring site in forming the intersubunit cross arm, which is apparently required for L2 binding.

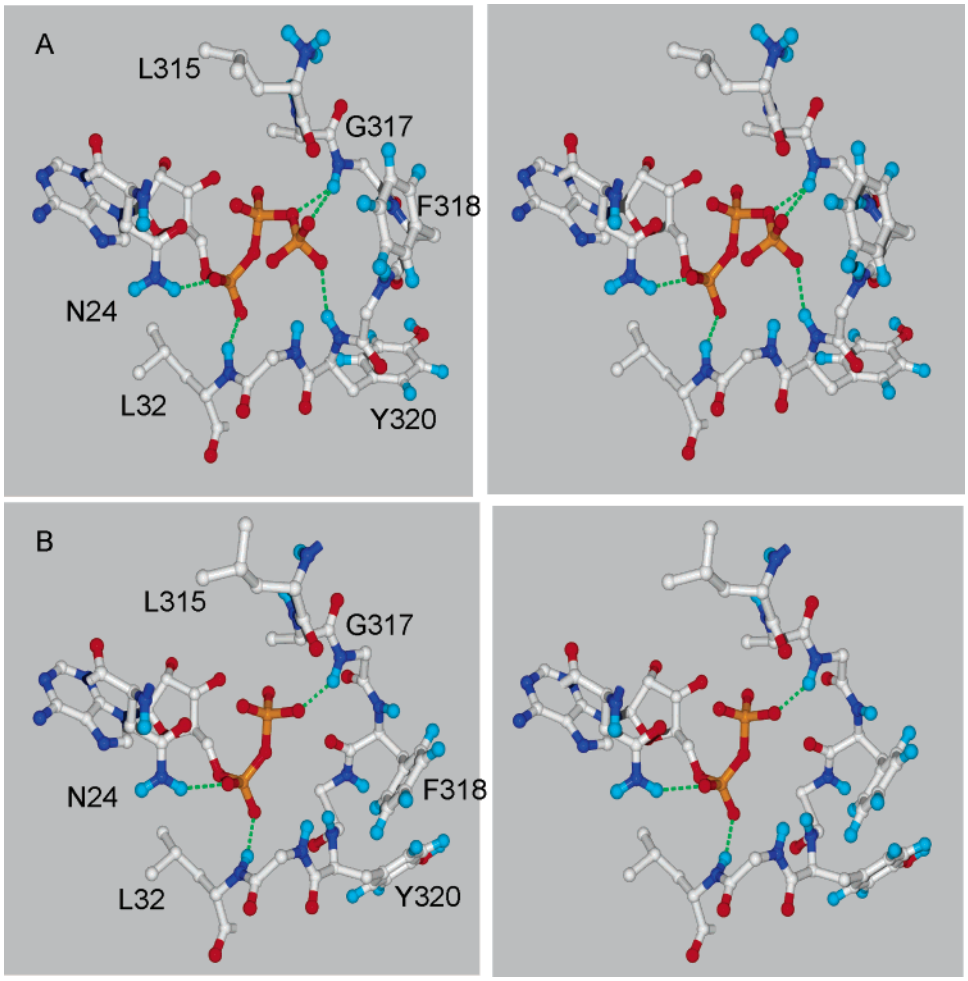


FIGURE 5: Stereoview showing differences in conformation and H-bond interactions of the ATP binding site of PDHK-2·ATP (panel A) bound and PDHK-2·ADP·DCA (panel B). H-bonds are indicated by dashed lines. In panel B, ** indicates the carbonyl group of Phe318 has moved into a position hindering ADP dissociation when both ADP and DCA are bound.

A common mode of binding ADP and ATP analogues was described for rat PDHK2 (*33*), BCK (*34*) and other members of the GHKL family (*36*−*38*, *41*, *73*, *75*). We report a fully defined ATP molecule rather than an ATP analogue bound at the active site. ATP bound to PDHK3·L2 was recently reported (*64*) and has some notable structural differences at the active site (below). The ATP, soaked into crystals of human PDHK2 in the presence of Nov3r, was not hydrolyzed. In contrast to when ADP/DCA are bound, the C-terminal cross arm interaction is maintained with just Nov3r bound or with ATP plus Nov3r or ATP bound. Binding of ATP is accompanied by binding of a $Mg^{2+}$ ion. Each phosphate group contributes one oxygen atom to the octahedral coordination of the $Mg^{2+}$ ion, which is completed by the Oδ1 atom of Asn247 and two water molecules (Figure 4). In apo PDHK2, the Glu243 carboxyl group is located where the α-phosphates of bound ATP/ADP reside. Supporting earlier proposals regarding the catalytic mechanism of PDHK2 (*33*, *75*, *76*), we observe a well-defined water molecule (Wat*, Figure 4) forming a water-mediated H-bond between the γ-phosphate and conserved Glu243. This water molecule occupies the position anticipated for the substrate serine residue. In the phosphoryl transfer reaction, Glu243 is proposed to act as a general base, aided by being polarized by His239 or Lys246 (*33*, *75*−*77*). Because of the proximity to the N-terminus of helix α12, the negative charges of the triphosphate are further compensated by the positive dipole moment of this helix.

While ATP and $Mg^{2+}$ are held in similar positions by PDHK3 and PDHK2, the PDHK3·ATP structure lacks water at the putative serine substrate position, and there are different H-bonding patterns with phosphates of ATP by residues 316−321 that enclose the reactive end of ATP (Figure 3S, Supporting Information). These differences in the disposition of the C-terminal end of the lid regions may be influenced by Nov3r bound to PDHK2 and differences in crystallization conditions, which in the case of PDHK3, led to $K^+$ being bound behind ATP within the active site entrance. Particularly different is the positioning of the carbonyl group of Gly319 which chelates $K^+$ in the case of PDHK3·ATP; this carbonyl group faces in nearly the opposite direction in PDHK2·ATP. The latter orientation in PDHK2 would appear to support forming an H-bond with the water located at the proposed position of the phosphorylated serine. It should be emphasized that, in the absence of potassium ion, PDHK2 has very high activity; $K^+$ substantially decreases the $K_m$ and $K_d$ for ATP along with decreasing $k_{cat}$ ($K_m/k_{cat}$ is unchanged) (*62*). This lid region also varies among the different PDHK2 (below) with impact on the apparent capacities to chelate $K^+$ (later section).

The backbone NH of Gly317 and Tyr320 form H-bonds to oxygen atoms of the γ-phosphate of ATP (Figure 5A)

with substantial repositioning of the Tyr320 side chain. The NH of Gly317 also forms an H-bond to the oxygen connecting to the $\gamma$ to the $\beta$-phosphate. There are substantial differences in the conformation of this loop with ADP bound compared with the rat PDHK2 (*33*) or with ADP bound along with DCA (Figure 5B). With just ADP bound (*33*), the NH's of Phe318 and Gly319 form good H-bonds with the $\beta$-phosphate of ADP. When DCA is bound along with ADP, the NH of Gly319 is positioned further away from the $\beta$-phosphate and the NH of Phe318 does not form an effective H-bond to an oxygen of the $\beta$-phosphate; however, the NH of Gly317 forms an H-bond to a $\beta$-phosphate oxygen. In the DCA/ADP structure, the C═O group (**, Figure 5B) of Phe318 moves next to $\beta$-phosphate, potentially hindering ADP dissociation (*52*, *62*).

*Binding of 3,3,3-Trifluoro-2-hydroxy-2-methylpropionates.* A series of 3,3,3-trifluoro-2-hydroxy-2-methylpropanoyl analogues have been described as potent PDHK inhibitors (*54*−*60*, *79*). Members of this class of inhibitors have been shown to lower blood glucose in insulin-resistant Zucker diabetic fatty rats (*78*). Although it has been reported that compounds of this class are not ATP-competitive (*57*), evidence has accumulated for a direct interaction of these inhibitors with PDHK (*59*). However, it was unclear how they interacted with PDHK.

We have determined the structure of PDHK2 in complex with two synthetic PDHK inhibitors of this class. The first is (4-{(2,5)-dimethyl-4-[3,3,3-trifluoro-2-hydroxy-2-methylpropanoyl]piperazinyl}carbonyl)benzonitrile (listed as 3r in ref *55* so designated as Nov3r here) and the second is (*N*-{4-[(ethylanilino)sulfonyl]-2-methylphenyl}-3,3,3-trifluoro-2-hydroxy-2-methylpropanamide); (example 12 in ref *82*, so designated as AZ12 here) and identified their common binding site (see Figure 1, residues marked with ‡). Both are potent inhibitors of PDHK2; the failure of Mann et al. (*58*) to detect potent inhibition of PDHK2 was due to the failure to include elevated $K^+$ which is required for observing inhibition of PDHK2 with EC50 of 5 nM with Nov3r.[4] These inhibitors bind the N-terminal domain of PDHK2 with the entry on the dimerization face of the R domain. This binding site (Figure 6) is formed by residues denoted ‡ in Figure 1. In both crystal structures, the (*R*)-3,3,3-trifluoro-2-hydroxy-2-methylpropionyl moiety of the ligands binds in a similar manner (Figure 6). Upon binding by Nov3r or AZ12A, helix $\alpha$2 shifts by a hinge motion around the C$\alpha$ position of Met25. This induces a 2−2.5 Å shift of the C$\alpha$ position of Phe31, and conformational change of its side chain from a lid position to open an induced pocket. The Phe31 side chain is located further in the binding site, alongside the bound inhibitor. The loop $\alpha$2−$\alpha$3 (residues 34−37) is found to be very flexible in all structures determined to date. This may be necessary to facilitate the hinge movement of helix $\alpha$2.

A key recognition feature is a hydrogen bond between the side chain hydroxyl of Ser41 and the 2-hydroxyl group of the ligands (Figure 6). The 2-methyl group extends into a small hydrophobic subpocket enclosed by residues Phe31, Ser41, Gln163, His164, Ile167, and Phe168. The trifluoromethyl group forms van der Waals interactions with the side chains of residues Phe44, Leu45, Phe28, Leu160, and Gln163. In the structure with Nov3r (Figure 6A), but not with AZ12 (Figure 6B), the side chain of Leu23 is also in contact with the trifluoromethyl group, to avoid steric clashes with its 2,6-dimethylpiperazine group. The amide oxygen of AZ12 forms a hydrogen bond to a buried water molecule, which bridges the backbone carbonyl of Phe28 and atom N$\epsilon$2 of Gln163. The central portion of the ligands is located in a short hydrophobic channel, formed by residues Leu23, Gln27, Phe28, Phe31, Ser41, and Phe44, connecting the (*R*)-3,3,3-trifluoro-2-hydroxy-2-methylpropionyl binding pocket with the protein surface. The 2,6-dimethylpiperazine moiety of Nov3r and the methylbenzyl group of AZ12 form hydrophobic interactions with the protein. The 4-cyanophenyl ketone of Nov3r and the *N*-benzyl-*N*-ethylsulfonamide of AZ12 point toward solvent and are partially disordered in the crystal structures, indicating their flexibility.

The residues interacting with these ligands are highly conserved in the four PDHK isoforms (green, Figure 1S, Supporting Information). Analysis of the aligned sequences of the four PDHK isozymes reveals that among the interacting residues in PDHK2, PDHK4 (GenBank accession U54617) (*20*) has only one residue difference. Aligned with Phe28, PDHK4 has a leucine (Leu32) in the equivalent position. Although Nov3r and AZ12 are potent inhibitors of PDHK2, like other inhibitors in this class (*59*), these inhibitors stimulated PDHK4 activity. The Leu substitution may contribute to the transformation from an inhibitory to a stimulatory response. Furthermore, a single nucleotide polymorphism (SNP) has been identified in some individuals resulting in a Leu32Phe exchange in PDHK4. Since Phe28 is directly involved in binding of Nov3r and AZ12 binding, this SNP could significantly influence the binding affinity of natural or synthetic ligands in effected PDHK4 variants.

*Nov3r and AZ12 Inhibitory Mechanism.* The binding site of Nov3r/AZ12 is in the end of the R domain most removed from the ATP binding site (Figure 2) with the entrance on the dimerization face of the R domain. No changes occurred in the Nov3r site upon binding of ATP; Nov3r did not prevent binding of ATP at the active site. These observations suggested that inhibition primarily results from a mechanism other than perturbation of the active site. The requirement for a specific lipoamide binding pocket within PDHKs raised an alternate inhibitory mechanism. It has been proposed that the reversible association of the enzyme with the flexible lipoyl domains of the E2 core enables a PDHK dimer to migrate over the surface of a PDC and to rapidly phosphorylate multiple E1 (*2*, *8*, *12*, *13*). Compounds that interfere with the interaction of PDHK with the E2 core of the PDC would greatly decrease kinase activity.

Although Nov3r-class compounds inhibit PDHK activity (*55*−*59*), particularly PDHK2 (*59*), Nov3r did not inhibit phosphorylation of a recombinant E1 substrate peptide (*58*). We confirmed this using biotinylated myelin basic protein as substrate (data not shown). Nov3r was found to inhibit E2-activated PDHK2 activity but only modestly inhibit the phosphorylation of free E1. Furthermore, Nov3r hinders binding of PDHK2 to the L2 domain.[4] The binding site of Nov3r and AZ12 consists of a polar anchoring region that is linked to the protein surface by a short hydrophobic

[4] Hu, L., Yan, X. Y., Hiromasa, Y., and Roche, T. E., manscript in preparation. Selective mutations within Nov3r binding site prevent stimulation by reductive acetylation and Nov3r prevents the binding of PDHK2 to GST-L2 and E2. Potent inhibition of PDHK2 by Nov3r requires elevated $K^+$ ion.

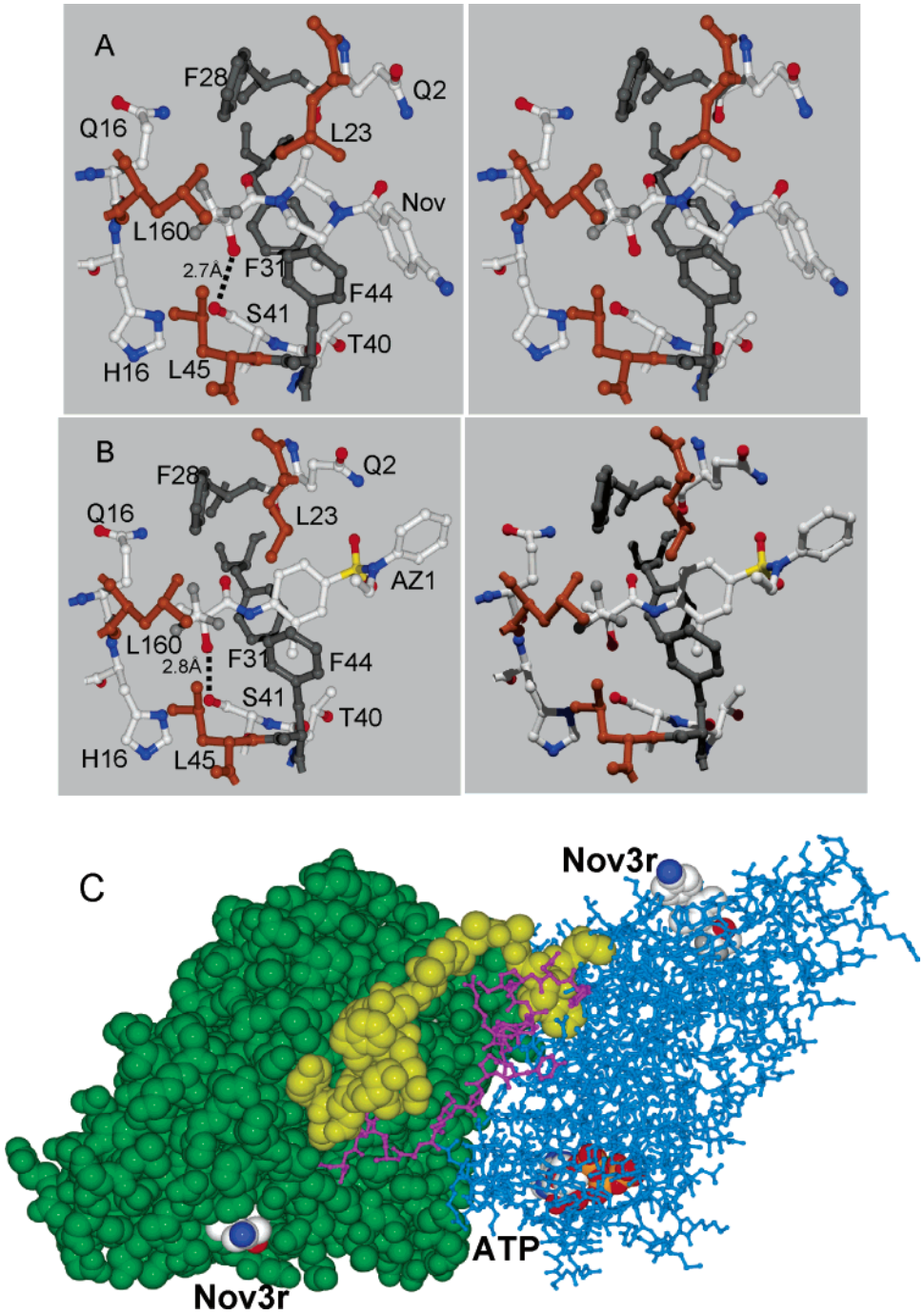


FIGURE 6: Stereoviews of Nov3r (panel A) and AZ12 (panel B) binding pocket in the N-terminal domain and PDHK2·Nov3r·ATP dimer with cross arm (panel C). In panels A and B, the inhibitors are shown in CPK. Panel C shows PDHK2·ATP·Nov3r dimer with left subunit in space filled format (cross arm in yellow green) and right subunit in sticks format (cross arm in magenta color).

channel. These properties could also be expected for the proposed binding site of the lipoamide group of the lipoyl domain. This observation and subsequent studies[4] raised the possibility that the binding site of Nov3r and AZ12 on the N-terminal domain of PDHK2 is the proposed lipoamide binding site. The recent studies of Kato et al. (*64*) present direct evidence with PDHK3 isoform for lipoyl binding at the corresponding site. Accordingly, this class of compounds acts as lipoamide antagonists that inhibit the E2-elevated ATP-dependent phosphorylation of E1 by blocking the association between PDHK and the L2 domain of the E2. The stimulation of PDHK4 by Nov3r-class inhibitors (*59*) demonstrates the potential for Nov3r binding site inducing changes causing stimulation at the distant active site. This stimulation of PDHK4 is likely to be related to the stimulation by reductively acetylated lipoyl groups of E2. With just Nov3r or AZ12 bound or with Nov3r and ATP bound, the cross arm is maintained (Figure 6C) and appears unchanged from the apo structure. Therefore, with or without the lipoyl binding site occupied, L2 domain binding is not required for formation and maintenance of the cross arm as could be implied from the PDHK3·L2 structures (*64*) alone.

*The DCA/Pyruvate Binding Site.* Pyruvate is an important physiological inhibitor of kinase activity that directly binds to PDHK (*80*). Several lines of evidence indicate that DCA and pyruvate bind at the same binding site. DCA and pyruvate show the same complex patterns of uncompetitive inhibition in the absence and noncompetitive inhibition of

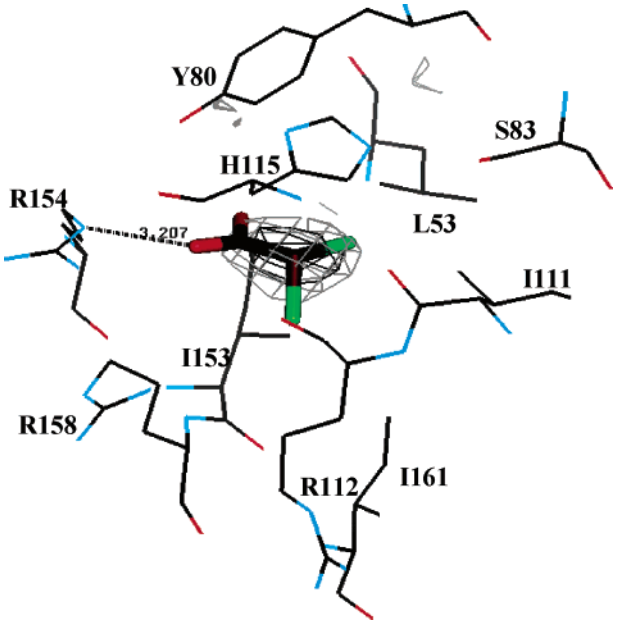


FIGURE 7: DCA interactions when bound by the N-terminal domain of human PDHK2·ADP. The model is superimposed onto the 2.5 Å $[f_{obs}(native) - f_{obs}(ADP,DCA)]\alpha_{calc}$ (native) difference electron density map contoured at $4\sigma$ (red) and $5\sigma$ (black). A H-bond between Arg154 and DCA in indicated by a broken line and its distance is labeled.

kinase activity in the presence of ADP (*52*). Both pyruvate and DCA enhance ADP binding relative to ATP (*52*, *62*). In mechanism studies, DCA is often used in place of pyruvate because DCA is not used by E1 to form acetylated lipoyl groups, a condition that stimulates kinase activity. The location of the pyruvate/DCA binding site has not been previously addressed. We therefore undertook experiments to identify the DCA/pyruvate binding site of human PDHK2, by soaking crystals of human PDHK2·ADP with high concentrations of DCA.

A DCA binding site was unambiguously identified by calculating a difference Fourier map. The map contains a peak greater than 5.5 $\sigma$ in a small pocket within the N-terminal domain of human PDHK2 (Figure 7). The pocket is formed by residues Leu53, Tyr80, Ser83, Ile111, Arg112, His115, Ser153, Arg154, Ile157, Arg158, and Ile161 ($\rho$ residues, Figure 1). Most of these residues are conserved among PDHK isoforms from different species (dark blue, Figure 1S, Supporting Information). The carboxylate group of DCA forms a salt-bridge with Arg154, while the two chlorine substituents are deeply buried in the hydrophobic portion of the pocket. DCA is sandwiched between His115 and Ile57. PDHK3 is poorly inhibited by DCA/pyruvate (*22*, *61*) and has a phenylalanine (Phe153) in place of Ile157. Molecular modeling studies with PDHK2 indicated that, upon I157F substitution, the Phe side chain and His115 would tend to fill in this site; introducing this mutation indeed led to loss of DCA and pyruvate inhibition.[4] Difference maps of crystals soaked with pyruvate support pyruvate binding at the same site as DCA (data not shown). However, due to lower data quality, the interpretation is not as conclusive as for DCA.

The DCA/pyruvate binding pocket is close to the surface of the extended groove of the active site cavity formed between the R and Cat domains with a cluster of conserved arginine residues (Arg112, Arg154, Arg158) on the R domain of the DCA site. As indicated above, Arg154 forms an electrostatic interaction with the carboxyl group of DCA. In the structure with DCA bound, Arg158 appears to block the entry to the DCA site. In the rat PDHK2·ADP structure, Arg158 moves to open up the site with the Arg158 side chain forming an interaction with Tyr328 side chain. Although enhanced binding of DCA (i.e., access to DCA site) is predicted when ADP is bound by kinetic studies (*62*), it is not clear whether the positioning of the Arg158 side chain is influenced by ADP binding.

DCA binding is predicted to hinder dissociation of ADP at the active site (*62*). When comparing PDHK2 structures with ADP bound (rat PDHK2 (*33*)) versus the structure containing both ADP and DCA, there are changes in how the 316−320 backbone NH form hydrogen bonds with the $\beta$-phosphate of ADP. Additionally, the carbonyl group of Phe318 appears to move in front of $\beta$-phosphate, which may hinder ADP dissociation in the latter structure.

Besides slowing ADP dissociation (*62*), DCA/pyruvate may inhibit the phosphorylation of the PDC, by interfering with the binding of PDHK to one of the components of the PDC, e.g., the L2 domain of E2 or the E1 substrate or both. Indeed, recent studies indicate that the combination of ADP plus pyruvate greatly hinder binding of PDHK2 to E2 component.[3] A potential mechanism for interfering with binding is to hinder cross arm formation and more specifically the interaction of Trp383 with the dimerization face of the N-terminal domain near the DCA/pyruvate site. The capacity of pyruvate plus ADP to strongly quench Trp fluorescence[3] is consistent with this interpretation.

*$K^+$ Site.* Human PDHK2 crystals were obtained from conditions with minimal $K^+$; however, $K^+$ has been shown to be important for strong ATP and ADP binding to PDHK2 as well as for pyruvate/DCA inhibition and stimulation by reductive acetylation of lipoyl groups (*62*, *63*). A $K^+$ site was observed in the structure of the related BCK when ADP was bound (*34*) and in PDHK3 structures (*64*). We have modeled a $K^+$ ion bound in an analogous position in PDHK2 crystal structures. Figure 8 compares three human PDHK2 structures with apo enzyme, ADP plus DCA, or ATP (and Nov3r) bound. In the apo enzyme the backbone carbonyl groups of Leu295, Gly319, and Ser297 along with the oxygen atom of the Ser301 hydroxyl are positioned so that they could chelate $K^+$ in this position. With ADP/DCA bound, these oxygen atoms are optimally positioned along with an oxygen of the $\beta$-phosphate of ADP to chelate a $K^+$ ion (Figure 9). Therefore, strong chelation may hinder ADP dissociation. In the rat PDHK2 structure with just ADP bound, the carbonyl Tyr300 rather than Ser301 hydroxyl oxygen is positioned so that it could engage in chelating $K^+$. With ATP bound, additional H-bonds are formed between the main chain of the 317−320 loop and the $\gamma$-phosphate of ATP. This results in a conformational change that disrupts the proposed $K^+$ binding site, specifically preventing the C═O of Gly319 interacting with the ion. These changes at the active site are consistent with function/regulation studies (*2*, *15*, *52*, *61*, *62*). Elevated $K^+$ lowers the $K_m$ for ATP and $K_i$ for ADP and fosters strong inhibition by ADP plus DCA, and apparently causes ADP dissociation to be rate limiting (*62*, *63*). Reversing the effects of $K^+$ and speeding ADP dissociation appears to be a central feature in stimulation of

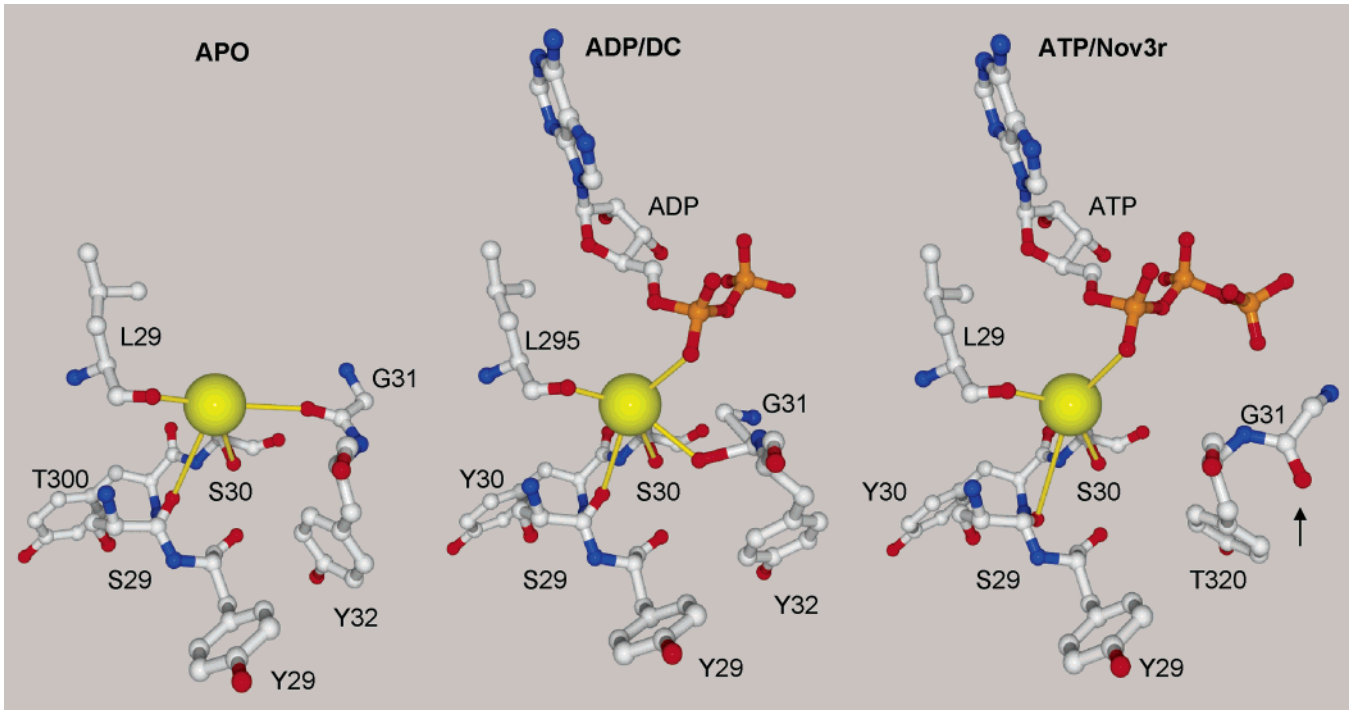


FIGURE 8: Enhanced capacity for $K^+$ binding with PDHK2·ADP·DCA as compared to PDHK2 or PDHK2·ATP·Nov3r structures. Using DeepViewPro-PdbViewer 3.7(SP5), the BCK structure (*34*) with AMP−PNP bound was superimposed with PDHK2·ATP·Nov3r and separately with PDHK2·ADP·DCA using "Iterative Magic Fit" in Deep-View program. The RMS were 1.46 and 1.48 Å for alignment of BCK with ATP- and ADP-containing PDHK2 structures, respectively. Then $K^+$ ion of BCK structure was merged into PDHK2 structures. The position of the $K^+$ was the same as the $K^+$ in PDHK3·ATP structure subsequently published (*64*).

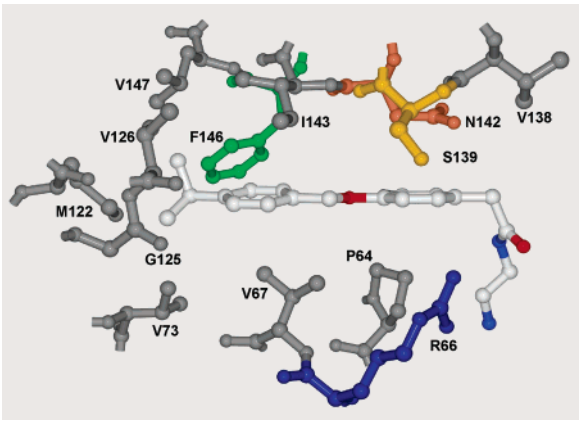


FIGURE 9: Binding site of Pfz3 on the regulatory domain of human PDHK2. Pfz3 (CPK representation). Residues interacting with Pfz3 are shown in ball-and-stick representation.

PDHK2 activity by reductive acetylation (*63*).

*Allosteric Regulation of the Kinase Activity*. High-throughput screening using a protein phosphorylation assay, has identified a PDHK inhibitor, (*N*-(2-aminoethyl)-2-{3-chloro-4-[(4-isopropylbenzyl)oxy]phenyl}acetamide), here designated Pfz3 (data not shown). Pfz3 inhibited kinase activity associated with porcine heart PDC with an EC50 of 2 $\mu$M. Soaking of crystals of human PDHK2 with Pfz3 led to the identification of an additional ligand binding site in the R domain of human PDHK2 (Figures 2 and 9). Because the binding site of Pfz3 is distant to the ATP-binding site and the proposed catalytic machinery, we postulate that Pfz3 inhibits PDHK2 by an allosteric mechanism.

The site, which is preformed in the native protein, is constituted by Leu63, Pro64, Arg66, Val67 of loop α3−α4 and helix α4, Ser72, Val73 of loop α4−α5 and helix α5, Met122, Gly125, Val126, Tyr129 of helix α7, Val138, Ser139, Asn142, Ile143, Phe146, Leu147 of loop α7−α8 and helix α8 as well as Tyr374 at the C-terminus of helix α13 († residues, Figure 1). The pocket is located at one end of the 4-helix bundle, opposite to the binding site of the 3,3,3-trifluoro-2-hydroxy-2-methylpropanoyl inhibitors described above. It is very lipophilic and extends approximately 15 Å into the core of the domain (Figure 9). Although this corresponds to the dimension of the extended lipoyl-lysine arm of the E2, we concluded that this site was not the lipoamide binding site of PDHK since the inhibition pattern of Pfz3 differs from that of exogenous L2 domain or the previously described 3,3,3-trifluoro-2-hydroxy-2-methylpropionates, in that Pfz3 decreased the rate of phosphorylation of peptide substrate (data not shown).

Fourteen out of the 20 amino acid residues forming this allosteric ligand binding site are conserved in all four human PDHK isozymes (cyan residues, Figure 1S, Supporting Information). Moreover, four of the nonconserved residues constituting the pocket (Val126, Val138, Ser139, Ile143) either make main-chain contributions or are replaced by homologous amino acids in at least one of the other PDHK isozymes, suggesting that these variations have little effect on the overall size and properties of the binding site. Thr70 is exterior to contact residues but contributes to enclosing the Pfz3 site; Thr70 is replaced by an arginine in human PDHK3. That change could significantly alter the polarity of the pocket, depending on the conformation of the side chain. Most importantly, however, Val67 is unique to human PDHK2. In human PDHK isozymes 1, 3, and 4, the corresponding residue is a leucine. Val67 side chain is located in the center of the Pfz3 pocket; the larger leucine side chain could severely restrict access to the binding pocket in human

PDHK isozymes other than isozyme 2. It may therefore be possible to design allosteric inhibitors that are specific for human PDHK2.

We have not observed any significant conformational differences between the structures of human PDHK2 in the presence or absence of Pfz3. We therefore cannot offer a conclusive theory on the mechanism of the allosteric inhibition of human PDHK2 by Pfz3. However, given the amino acid variation on the inner surface of this binding pocket, it is tempting to speculate that physiological effectors could bind in an isozyme-specific manner, thereby modulating PDHK activity depending on the isozyme prevalence in different tissues. One candidate for a physiological effector is CoA. Pfz3 resembles the functional end of CoA, which directly inhibits PDHK2 activity (*62*). In the presence of saturating Pfz3, there is no additional inhibition of human PDHK2 by saturating level of CoA.[4] That moiety of Pfz3 protrudes from the dimerization face of R domain of PDHK2 alongside Tyr374. That area is presumed to be the entry site for Pfz3. However, for CoA to bind at this site, it would have to enter from the other side of the R domain and this would place the adenine portion of CoA close to the active site. Pfz3 points at a well ordered Va126 at the other end but a potential opening toward the end of the helices of the R domain occurs at Glu128. Glu128 would have to be displaced by the phosphate groups of CoA in order for the other end of CoA to bind in a fashion analogous to Pfz3. Further studies will be needed to evaluate this possibility.

*Final Considerations.* PDHK is a dimeric mitochondrial protein kinase, consisting of an N-terminal four-helix bundle and a C-terminal catalytic domain. In this study we report the crystal structures[2] of human PDHK2 in the presence of ATP and with three different classes of inhibitors: lipoamide antagonists, dichloroacetate and an allosteric kinase inhibitor. None of these inhibitors binds at the ATP/ADP site of PDHK, but instead they bind at different sites on the N-terminal domain. We, therefore, have demonstrated that the N-terminal domain of PDHK2 has a key regulatory function and contains at least three distinct binding sites and have termed this the R domain. We have shown that a stable C-terminal cross arm forms in human PDHK2 that is retained with ATP and Nov3r bound but not when ADP and DCA are bound.

By obtaining a structure with a bound ATP, we have expanded understanding of the active site. Significant differences are found when ADP, ATP, and ADP with DCA are bound. We suggest an interacting $K^+$ ion may explain the critical requirement for elevated $K^+$ for all regulatory effects (*62*, *63*). The structures we have determined help to explain the different modes of inhibition displayed by the different inhibitor classes. The finding of three previously unidentified ligand binding sites with apparent pharmacological relevance, in addition to the known ATP/ADP binding site, greatly enhances the opportunities to modulate the activity of PDHK in an isozyme and tissue specific manner. Most importantly, the structures can be used as a tool for structure based design of PDHK inhibitors.

## SUPPORTING INFORMATION AVAILABLE

Aligned sequences of mature sequences of human PDHK (Figure 1S); PDHK2 and PDHK3 structure overlap (Figure 2S); stereoviews of PDHK2 and PDHK3 interactions with ATP (Figure 3S). This material is available free of charge via the Internet at http://pubs.acs.org.

## REFERENCES


1. Patel, M. S., and Roche, T. E. (1990). Molecular biology and biochemistry of pyruvate dehydrogenase complexes, *FASEB. J. 4*, 3224−3233.
2. Roche, T. E., Baker, J., Yan, X., Hiromasa, Y., Gong, X., Peng, T., Dong, J., Turkan, A., and Kasten, S. A. (2001) Distinct regulatory properties of pyruvate dehydrogenase kinase and phosphatase isoforms, *Prog. Nucleic Acid Res. Mol. Biol. 70*, 33−75.
3. Yeaman, S. J., Hutcheson, E. T., Roche, T. E., Pettit, F. H., Brown, J. R., Reed, L. J., Watson, D. C., and Dixon, G. H. (1978) Sites of phosphorylation on pyruvate dehydrogenase from bovine kidney and heart, *Biochemistry 17*, 2364−2370.
4. Korotchkina, L. G., and Patel, M. S. (1995) Mutagenesis studies of the phosphorylation sites of recombinant human pyruvate dehydrogenase, site-specific regulation, *J. Biol. Chem. 270*, 14297−14304.
5. Kolobova, E., Tuganova, A., Boulatnikov, I., and Popov, K. M. (2001) Regulation of pyruvate dehydrogenase activity through phosphorylation at multiple sites, *Biochem. J. 358*, 69−77.
6. Patel, M. S., and Korotchkina, L. G. (2001) Regulation of mammalian pyruvate dehydrogenase complex by phosphorylation: complexity of multiple phosphorylation sites and kinases, *Exp. Mol. Med. 33*, 191−197.
7. Ono, K., Radke, G. A., Roche, T. E., and Rahmatullah, M. (1993) Partial activation of the pyruvate dehydrogenase kinase by the lipoyldomain region of E2 and interchange of the kinase between lipoyl domain regions, *J. Biol. Chem. 268*, 26135−26143.
8. Liu, S., Baker, J. C., and Roche, T. E. (1995) Binding of the pyruvate dehydrogenase kinase to recombinant constructs containing the inner lipoyl domain of the dihydrolipoyl acetyltransferase component, *J. Biol. Chem. 270*, 793−800.
9. Yang, D., Gong, X., Yakhnin, A., and Roche, T. E. (1998) Requirements for the adaptor protein role of dihydrolipoyl acetyltransferase in the upregulated function of the pyruvate dehydrogenase kinase and pyruvate dehydrogenase phosphatase, *J. Biol. Chem. 273*, 14130−14137.
10. Jackson, J. C., Vinluan, C. C., Dragland, C. J., Sundararajan, V., Yan, B., Gounarides, J. S., Nirmala, N. R., Topiol, S., Ramage, P., Blume, J. E., Aicher, T. D., Bell, P. A., and Mann, W. R. (1998) Heterologously expressed inner lipoyl domain of dihydrolipoyl acetyltransferase inhibits ATP-dependent inactivation of pyruvate dehydrogenase complex, Identification of important amino acid residues, *Biochem. J. 334*, 703−711.
11. Tuganova, A., Boulantnikov, I., and Popov, K. M. (2002) Interaction between the individual isoenzymes of pyruvate dehydrogenase kinase and the inner lipoyl-bearing domain of transacetylase component of pyruvate dehydrogenase complex, *Biochem. J. 366*, 129−136.
12. Hiromasa, Y., and Roche, T. E. (2003) Facilitated interaction between the pyruvate dehydrogenase kinase isoform 2 and the dihydrolipoyl acetyltransferase, *J. Biol. Chem. 278*, 33681−33693.
13. Roche, T. E., Hiromasa, Y., Turkan, A., Gong, X., Peng, T., Yan, X., Kasten, S. A., Bao, H., and Dong, J. (2003) Essential roles of lipoyl domains in the activated function and control of pyruvate dehydrogenase kinases and phosphatase isoform 1, *Eur. J. Biochem. 270*, 1050−1056.
14. Radke, G. A., Ono, K., Ravindran, S., and Roche, T. E. (1993) Critical role of a lipoyl cofactor of the dihydrolipoyl acetyltransferase in the binding and enhanced function of the pyruvate dehydrogenase kinase, *Biochem. Biophys. Res. Commun. 190*, 982−991.
15. Cate, R. L., and Roche, T. E. (1978) A unifying mechanism for stimulation of mammalian pyruvate dehydrogenase kinase activity by NADH, dihydrolipoamide, acetyl-CoA, or pyruvate, *J. Biol. Chem. 253*, 496−503.
16. Rahmatullah, M., and Roche, T. E. (1985) Modification of bovine kidney pyruvate dehydrogenase kinase activity by CoA esters and their mechanism of action, *J. Biol. Chem. 260*, 10146−10152.
17. Ravindran, S., Radke, G. A., Guest, J. R., and Roche, T. E. (1996) Lipoyl domain-based mechanism for the integrated feedback

control of the pyruvate dehydrogenase complex by enhancement of pyruvate dehydrogenase kinase activity, *J. Biol. Chem. 271*, 653−662.
18. Popov, K. M. (1997) Regulation of mammalian pyruvate dehydrogenase kinase, *FEBS Lett. 419*, 197−200.
19. Guidi, R., Bowker-Kinley, M. M., Kedishvili, N. Y., Zhao, Y., and Popov, K. M. (1995) Diversity of the pyruvate dehydrogenase kinase gene family in humans, *J. Biol. Chem. 270*, 28989−28994.
20. Rowles, J., Scherer, S. W., Xi, T., Majer, M., Nickle, D. C., Rommens, J. M., Popov, K. M., Harris, R. A., Riebow, N. L., Xia, J., Tsui, L.-C., Bogardus, C., and Prochazka, M. (1996) Cloning and characterization of PDHK4 on 7q21.3 encoding a fourth pyruvate dehydrogenase kinase isozyme in human, *J. Biol. Chem. 271*, 22376−22382.
21. Huang, B., Gudi, R., Wu, P., Harris, R. A., Hamilton, J. and Popov, K. M. (1998) Isozymes of pyruvate dehydrogenase phosphatase. DNA-derived amino acid sequences, expression, and regulation, *J. Biol. Chem. 273*, 17680−17688.
22. Bowker-Kinley, M. M., Davis, W. I., Wu, P., Harris, R. A., and Popov, K. M. (1998) Evidence for existence of tissue-specific regulation of the mammalian pyruvate dehydrogenase complex, *Biochem. J. 329*, 191−196.
23. Wu, P., Blair, P. V., Sato, J., Jaskiewicz, J., Popov, K. M., and Harris, R. A. (2000) Starvation increases the amount of pyruvate dehydrogenase kinase in several mammalian tissues, *Arch. Biochem. Biophys. 381*, 1−7.
24. Harris, R. A., Huang, B., and Wu, P. (2001) Control of pyruvate dehydrogenase kinase gene expression, *Adv. Enzymol. Regul. 41*, 269−288.
25. Sugden, M. C., Bulmer, K., and Holness, M. J. (2001) Fuel-sensing mechanisms integrating lipid and carbohydrate utilization, *Biochem. Soc. Trans. 29*, 272−278.
26. Holness, M. J., Kraus, A., Harris, R. A., and Sugden, M. C. (2000) Targeted upregulation of pyruvate dehydrogenase kinase (PDHK)-4 in slow-twitch skeletal muscel undrelies stable mosdification of the regulatory characteristics of PDHK induced by fat feeding, *Diabetes 49*, 775−781.
27. Wu, P., Peters, J. M., and Harris, R. A. (2001) Adaptive increase in pyruvate dehydrogenase kinase 4 during starvation is mediated by peroxisome proliferator-activated receptor α, *Biochem. Biophys. Res. Commun. 287*, 391−396.
28. Huang, B., Wu, P., Bowker-Kinley, M. M., and Harris, R. A. (2002) Regulation of pyruvate dehydrogenase kinase expression by peroxisome proliferator-activated receptor-α ligands, glucocorticoids, and insulin, *Diabetes 51*, 276−283.
29. Huang, B., Wu, P., Popov, K. M., and Harris, R. A. (2003) Starvation and diabetes reduce the amount of pyruvate dehydrogeanse phosphatase in rat heart and kidney, *Diabetes 52*, 1371−1376.
30. Harris, R. A., Popov, K. M., Zhao, Y., Kedishvili, N. Y., Shimomura, Y., and Crabb, D. W. (1995) A new family of protein kinases—the mitochondrial protein kinases, *Adv. Enzyme Regul. 35*, 147−162.
31. Bower-Kinley, M., and Popov, K. M. (1999) Evidence that pyruvate dehydrogenase kinase belongs to the ATPase/kinase superfamily, *Biochem. J. 344*, 47−53.
32. Wynn, R. M., Chaung, J. L., Cote, C. D., and Chuang, D. T. (2000) Tetrameric assembly and conservation in the ATP-binding domain of rat branched-chain alpha-ketoacid dehydrogenase kinase, *J. Biol. Chem. 275*, 30512−30519.
33. Steussy, C. N., Popov, K. M., Bowker-Kinley, M. M., Sloan, R. B., Jr., Harris, R. A., and Hamilton, J. A. (2001) Structure of pyruvate dehydrogenase kinase. Novel folding pattern for a serine protein kinase, *J. Biol. Chem. 276*, 37443−37450.
34. Machius, M., Chuang, J. L., Wynn, R. M., Tomchick, D. R., and Chuang, D. T. (2001) Structure of rat BCK kinase: nucleotide-induced domain communication in a mitochondrial protein kinase, *Proc. Natl. Acad. Sci. U.S.A. 98*, 11218−11223.
35. Dutta, R., and Inouye, M. (2000) GHKL, an emergent ATPase/kinase superfamily, *Trends Biochem. Sci. 25*, 24−28.
36. Wigley, D. B., Davies, G. J., Dodson, E. J., Maxwell, A., and Dodson, G. (1991) Crystal structure of an N-terminal fragment of the DNA gyrase B protein, *Nature 351*, 624−629.
37. Brino, L., Urzhumtsev, A., Mousli, M., Bronner, C., Mitschler, A., Oudet, P., and Moras, D. (2000). Dimerization of *Escherichia coli* DNA-gyrase B provides a structural mechanism for activating the ATPase catalytic center. *J. Biol. Chem. 275*, 9468−9475.
38. Obermann, W. M., Sondermann, H., Russo, A. A., Pavletich, N. P., and Hartl, F. U. (1998). In vivo function of Hsp90 is dependent on ATP binding and ATP hydrolysis, *J. Cell Biol. 143*, 901−910.
39. Tanaka, T., Saha, S. K., Tomomori, C., Ishima, R., Liu, D., Tong, K. I., Park, H., Dutta, R., Qin, L., Swindells, M. B., Yamazaki, T., Ono, A. M., Kainosho, M., Inouye, M., and Ikura, M. (1998) NMR structure of the histidine kinase domain of the *E. coli* osmosensor EnvZ, *Nature 396*, 88−92.
40. Bilwes, A. M., Alex, L. A., Crane, B. R., and Simon, M. I. (1999). Structure of CheA, a signal-transducing histidine kinase, *Cell 96*, 131−141.
41. Ban, C., Junop, M., and Yang, W. (1999) Transformation of MutL by ATP binding and hydrolysis: a switch in DNA mismatch repair, *Cell 97*, 85−97.
42. Whitehouse, S., Cooper, R. H., and Randle, P. J. (1974) Mechanism of activation of pyruvate dehydrogenase by dichloroacetate and other halogenated carboxylic acids, *Biochem. J. 141*, 761−774.
43. Bersin, R. M., and Stacpoole, P. W. (1977) Dichloroacetate as metabolic therapy for myocardial ischemia and failure, *Am. Heart J. 134*, 841−855.
44. Stacpoole, P. W., Henderson, G. N., Yan, Z., Cornett, R., and James, M. O. (1998) Pharmacokinetics, metabolism and toxicology of dichloroacetate, *Drug. Metab. Rev. 30*, 499−539.
45. Stacpoole, P. W., Henderson, G. N., Yan, Z., and James, M. O. (1998). Clinical pharmacology and toxicology of dichloroacetate, *Environ. Health Perspect. 106 Suppl 4*, 989−994.
46. Stacpoole, P. W. (1989) The pharmacology of dichloroacetate, *Metabolism 38*, 1124−1144.
47. Henderson, G. N., Curry, S. H., Derendorf, H., Wright, E. C., and Stacpoole, P. W. (1997). Pharmacokinetics of dichloroacetate in adult patients with lactic acidosis, *J. Clin. Pharmacol. 37*, 416−425.
48. Bersin, R. M., and Stacpoole, P. W. (1997). Dichloroacetate as metabolic therapy for myocardial ischemia and failure, *Am. Heart J. 134*, 841−855.
49. Greenhaff, P. L., Campbell-O'Sullivan, S. P., Constantin-Teodosiu, D., Poucher, S. M., Roberts, P. A., and Timmons, J. A. (2002) An acetyl group deficit limits mitochondrial ATP production at the onset of exercise, *Biochem. Soc. Trans. 30*, 275−280.
50. Wolff, A. A., Rotmensch, H. H., Stanely, W. C., and Ferrari, R. (2002) Metabolic approaches to the treatment of ischemic heart disease: the clinicians' perspective, *Heart Failure Rev. 7*, 187−203.
51. Lloyd, S., Brocks, C., and Chatham, J. C. (2003) Differential modulation of glucose, lactate, and pyruvate oxidation by insulin and dichloroacetate in the rat heart. *Am. J. Physiol. Heart Circ. Physiol. 285*, 163−172.
52. Pratt, M. L., and Roche, T. E. (1979) Mechanism of pyruvate inhibition of kidney pyruvate dehydrogenase$_a$ kinase and synergistic inhibition by pyruvate and ADP, *J Biol. Chem. 254*, 7191−7196.
53. Espinal, J., Leesnitzer, T., Hassman, A., Beggs, M., and Cobb, J. (1995). Inhibition of pyruvate dehydrogenase kinase by halogenated acetophones, *Drug Dev. Res. 35*, 130−136.
54. Aicher, T. D., Damon, R. E., Koletar, J., Vinluan, C. C., Brand, L. J., Gao, J., Shetty, S. S., Kaplan, E. L., and Mann, W. R. (1999) Triterpene and diterpene inhibitors of pyruvate dehydrogenase kinase (PDHK), *Bioorg. Med. Chem. Lett. 9*, 2223−2228.
55. Aicher, T. D., Anderson, R. C., Bebernitz, G. R., Coppola, G. M., Jewell, C. F., Knorr, D. C., Liu, C., Sperbeck, D. M., Brand, L. J., Strohschein, R. J., Gao, J., Vinluan, C. C., Shetty, S. S., Dragland, C., Kaplan, E. L., DelGrande, D., Islam, A., Liu, X., Lozito, R. J., Maniara, W. M., Walter, R. E., and Mann, W. R. (1999) (*R*)-3,3,3-Trifluoro-2-hydroxy-2-methylpropionamides are orally active inhibitors of pyruvate dehydrogenase kinase, *J. Med. Chem. 42*, 2741−2746.
56. Aicher, T. D., Anderson, R. C., Gao, J., Shetty, S. S., Coppola, G. M., Stanton, J. L., Knorr, D. C., Sperbeck, D. M., Brand, L. J., Vinluan, C. C., Kaplan, E. L., Dragland, C. J., Tomaselli, H. C., Islam, A., Lozito, R. J., Liu, X., Maniara, W. M., Fillers, W. S., DelGrande, D., Walter, R. E., and Mann, W. R. (2000) Secondary amides of (*R*)-3,3,3-trifluoro-2-hydroxy-2-methylpropionic acid as inhibitors of pyruvate dehydrogenase kinase, *J. Med. Chem. 43*, 236−249.
57. Bebernitz, G. R., Aicher, T. D., Stanton, J. L., Gao, J., Shetty, S. S., Knorr, D. C., Strohschein, R. J., Tan, J., Brand, L. J., Liu, C., Wang, W. H., Vinluan, C. C., Kaplan, E. L., Dragland, C. J.,

DelGrande, D., Islam, A., Lozito, R. J., Liu, X., Maniara, W. M., and Mann, W. R. (2000) Anilides of (*R*)-trifluoro-2-hydroxy-2-methylpropionic acid as inhibitors of pyruvate dehydrogenase kinase, *J. Med. Chem. 43*, 2248−2257.
58. Mann, W. R., Dragland, C. J., Vinluan, C. C., Vedananda, T. R., Bell, P. A., and Aicher, T. D. (2000) Diverse mechanisms of inhibition of pyruvate dehydrogenase kinase by structurally distinct inhibitors, *Biochim. Biophys. Acta 1480*, 283−292.
59. Morrell, J. A., Orme, J., Butlin, R. J., Roche, T. E., Mayers, R. M., and Kilgour, E. (2003) AZD7545 is a selective inhibitor of pyruvate dehydrogenase kinase 2. *Biochem. Soc. Trans. 31*, 1168−1170.
60. Mayers, R. M., Butlin, R. J., Kilgour, E., Leighton, B., Martin, D., Myatt, J., Orem, J. P., and Holloway, B. R. (2003) AZD7545, a novel inhibitor of PDHK2, activates PDH in vivo and improves blood glucose control in obese (fa/fa) Zucker rats. *Biochem. Soc. Trans. 31*, 1171−1173.
61. Baker, J. C., Yan, X., Peng, T., Kasten, S. A., and Roche, T. E. (2000) Marked differences between two isoforms of human pyruvate dehydrogenase kinase. *J. Biol. Chem. 275*, 15773−15781.
62. Bao, H., Kasten, S. A., Yan, X., and Roche, T. E. (2004) Pyruvate dehydrogenase kinase isoform 2 activity limited and further inhibited by slowing down the rate of dissociation of ADP, *Biochemistry 43*, 13432−13441.
63. Bao, H., Kasten, S. A., Yan, X., and Hiromasa, Y., and Roche, T. E. (2004) Pyruvate dehydrogenase kinase isoform 2 activity stimulated by speeding up the rate of dissociation of ADP, *Biochemistry 43*, 13442−13451.
64. Kato, M., Chuang, J. L., Tso, S.-C., Wynn, R. M. and Chuang, D. T. (2005) The Crystal structure of pyruvate dehydrogenasekinase 3 bound to lipoyl domain 2 of human pyruvate dehydrogenase complex, *EMBO J. 24*, 1763−1774.
65. Otwinowski, Z., and Minor, W. (1997) Processing of X-ray diffraction data collected in oscillation mode, *Methods Enzymol. 276*, 307−326.
66. Collaborative Computational Project, N. (1994). The CCP4 Suite: Programs for protein crystallography, *Acta Crystallogr., Sect. D 50*, 760−763.
67. de La Fortelle, E., and Bricogne, G. (1997) Maximum-likelihood heavy-atom parameter refinement for multiple isomorphous replacement and multiwavelength anomalous diffraction methods, *Methods Enzymol. 276*, 472−494.
68. Abrahams, J., and Leslie, A. (1996). Methods used in the structure determination of bovine mitochondrial $F_1$ ATPase, *Acta Crystallogr., Sect. D 52*, 30−42.
69. Accelrys Inc. (2000) Quanta, version 2000.1 ed, Accelrys Inc., San Diego, CA 92121-3752.
70. Accelrys Inc. (2002) CNX, version 2002.02 ed, Accelrys Inc., San Diego, CA 92121-3752.
71. Popov, K. M., Zhao, Y., Shimomura, Y., Kuntz, M. J. and Harris, R. A. (1992) Branched-chain α-ketoacid dehydrogenase kinase: Molecular cloning, expression, and sequence similarity with histidine protein kinases, *J. Biol. Chem. 267*, 13127−13130.
72. Tuganova, A., and Popov, K. M. (2005) Role of protein−protein interactions in the regulation of pyruvate dehydrogenase kinase, *Biochem. J. 387*, 147−153.
73. Boulatnikov, I., and Popov, K. M. (2003) Formation of functional heterodimers by isozymes 1 and 2 of pyruvate dehydrogenase kinase, *Biochim. Biophys. Acta 1645*, 183−192.
74. Prodromou, C., Roe, S. M., O'Brien, R., Ladbury, J. E., Piper, P. W., and Pearl, L. H. (1997) Identification and structural characterization of the ATP/ADP-binding site in the Hsp90 molecular chaperone, *Cell 90*, 65−75.
75. Tuganova, A., Yoder, M. D., and Popov, K. M. (2001) An essential role of Glu-243 and His-239 in the phosphotransfer reaction catalyzed by pyruvate dehydrogenase kinase, *J. Biol. Chem. 276*, 17994−17999.
76. Popov, K. M., Tuganova, A., Bowker-Kinley, M. M., Hung, B., Wu, P., Steussy, C. N., Hamilton, J., and Harris, R. A. (2004) Structure, Function, and Regulation of Pyruvate Dehydrogenase Kinase, in *Thiamine, Catalytic Mechanisms in Normal and Disease States* (Jordan, F., and Patel, M. S., Eds.) Marcel Dekker, Inc., New York.
77. Tovar-Mendez, A., Hirani, T. A., Miernyk, J. A., and Randall, D. D. (2005) Analysis of the catalytic mechanism of pyruvate dehydrogenase kinase, *Arch. Biochem. Biophys. 434*, 159−168.
78. Mayers, R. M., Leighton, B., and Kilgour, E. (2005) PDH kinase inhibitors: a novel therapy for Type II diabetes, *Biochem. Soc. Trans. 33*, 367−370.
79. Butlin, R. J., and Burrows, J. N. (1999) Patent WO-1999-9962873 A1 Benzenesuphonamide derivatives as pyruvate dehydrogenase activators, Zeneca Limited.
80. Hucho, F., Randall, D. D., Roche, T. E., Burgett, M. W., Pelley, J. W., and Reed, L. J. (1972) α-keto acid dehydrogenase complexes. XVII. Kinetic and regulatory properties of pyruvate dehydrogenase kinase and pyruvate dehydrogenase phosphatase from bovine kidney and heart, *Arch. Biochem. Biophys. 151*, 328−340.

BI051402S